Applied Ocean Research 164 (2025) 104791

Contents lists available at ScienceDirect

Applied Ocean Research

journal homepage: www.elsevier.com/locate/apor

Invited paper

Multi-purpose offshore wind: A case study on integrating passive acoustic surveillance into infrastructure in the North Sea

Magnus Ferris [a], Edward Clark [a,b], Guillermo Jiménez Arranz [c], Philippe Blondel [c], Cormac Reale [d], Alan Hunter [a], Anna Young [a,*]

[a] Department of Mechanical Engineering, United Kingdom
[b] Department of Computer Science, United Kingdom
[c] Department of Physics, United Kingdom
[d] Department of Architecture and Civil Engineering, University of Bath, Bath, United Kingdom

ARTICLE INFO

Keywords:
Offshore renewable energy
Underwater acoustics
Acoustic detection
Acoustic surveillance

ABSTRACT

This study investigates the feasibility and effectiveness of integrating acoustic sensors into offshore renewable energy infrastructure for multi-purpose underwater monitoring, with a focus on detecting illegal fishing activity. Two North Sea sites (Dogger Bank and Buchan Deep) were analysed to assess acoustic detection capabilities over a frequency bandwidth from 100 Hz to 10 kHz. The main uncertainties in the modelling stem from limited knowledge of the sediment properties, and from the range of possible source levels. The work could therefore be expanded by considering a stochastic approach to these uncertainties if a specific site was taken forward for trials of the monitoring method. The results indicate that a single hydrophone attached to the turbine substructure can detect the activity of a fishing vessel within a range of 300 to 400 m under average conditions, extending up to 2 to 4 km under favourable conditions. Optimal detection frequencies were typically in the range of 500 Hz to 5 kHz.

Detection performance is strongly influenced by ambient noise levels and sediment composition, while water depth has minimal impact. Seasonal variations significantly affect sound propagation, with a downward-refracting sound speed profile in the summer and attenuating sediments increasing propagation loss. This increased loss is offset by reduced ambient noise due to calmer sea states, resulting in longer detection ranges during the summer. The optimistic detection ranges align with or exceed typical turbine spacing, suggesting that a hydrophone-equipped wind farm could effectively monitor fishing activity across its footprint. Coverage would not extend beyond its boundaries into adjacent Marine Protected Areas.

1. Introduction

The UK is a world leader in the development and adoption of offshore renewable energy (ORE) with almost 14 GW of offshore wind capacity installed across 51 different sites (see Table 1). This represents 40% of the total installed capacity in Europe (Burton et al., 2021). In 2024, the UK generated 17% of its electricity needs from offshore renewables (second only to Denmark in Europe WindEurope, 2025), a number which is set to grow as fossil fuels are progressively phased out to meet net-zero targets (TCE, 2022). The 2022 British Energy Security Strategy has set a target of 50 GW of installed offshore capacity by 2030 (GOV.UK, 2022), and currently there is 7.6 GW under construction. Beyond 2030, the Climate Change Committee has set a net-zero target by 2050 of up to 140 GW of offshore energy. While this target represents a considerable challenge, the UK is rising to it with over 50 GW planned in the current development cycle, see Table 1.

While the primary purpose of this infrastructure is and will continue to be energy production, this "ORE archipelago" offers a unique opportunity as a marine sensing network for minimal additional expenditure. The currently installed and planned archipelago extends over much of the UK Eastern seaboard allowing for its near-complete marine sensing coverage if instrumented, see Fig. 1. Potential marine sensing opportunities include but are not limited to detecting: the presence of smuggling; unsanctioned intrusions by foreign powers into sovereign waters; illegal fishing in protected waters (Appleby et al., 2020); the impacts of offshore infrastructure on marine habitats and fish populations (Bald, 2022); changes in the structural integrity of the turbine sub- and superstructure (Prendergast et al., 2018).

If ORE infrastructure were routinely instrumented and the data made available, the following parties would benefit: Researchers would

* Corresponding author.
E-mail address: amy32@bath.ac.uk (A. Young).

https://doi.org/10.1016/j.apor.2025.104791
Received 2 July 2025; Received in revised form 28 August 2025; Accepted 29 September 2025
Available online 4 October 2025

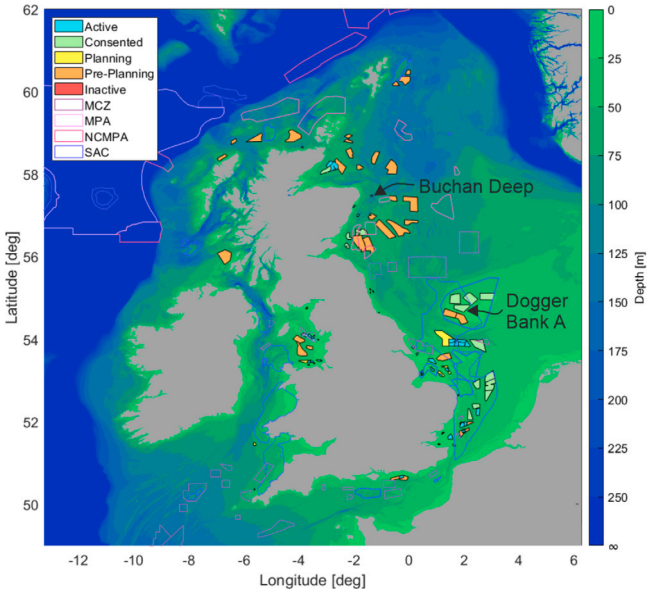

Fig. 1. Map of active and planned offshore wind farms in the UK, with the selected case study sites labelled. The limits of UK/EU marine protected areas are shown as coloured lines. The acronyms refer to Marine Conservation Zone (MCZ), Marine Protected Area (MPA), Natural Conservation Marine Protected Area (NCMPA), and Special Area of Conservation (SAC). (For interpretation of the references to colour in this figure legend, the reader is referred to the web version of this article.)
Sources: Bathymetry from GEBCO 2022 grid (GEBCO, 2022), Scottish OWF sites from Crown Estate Scotland Spatial Hub (CES, 2024), OWF sites in England, Wales and Northern Ireland from The Crown Estate Open Data Portal (TCE, 2024), and MPAs from UK Offshore Marine Protected Areas (JNCC, 2023).

have access to data to analyse the performance, efficiency, and environmental impacts of offshore renewable projects, leading to further advancements in the field. Energy companies would better understand the operational performance of their assets, leading to optimal energy production, pre-emptive identification of maintenance needs and overall improvements in efficiency. Environmental organisations could monitor the impact of ORE infrastructure on marine ecosystems and wildlife, informing future sustainable development practices. Regulatory bodies could use the data to support evidence-based decision-making for the expansion of offshore renewable projects. Financial institutions could use the data to de-risk future green energy investment, hastening the green energy transition. Defence agencies could augment their existing data to ensure energy security and protection of sovereign waters.

This paper seeks to initiate research in this field by exploring the potential benefits of installing acoustic sensors on existing ORE infrastructure. In particular, the paper focuses on quantifying the likely detection ranges of a commercially-available hydrophone mounted on a wind turbine foundation, and considers a fishing vessel as the acoustic source. The approach was trialled using data from the Dogger Bank wind turbine farm - a Marine Protected Area with a history of illegal fishing (Appleby et al., 2020) - and from the Buchan Deep - the site of the UK's first commercial-scale floating wind turbine. The work uses established techniques and models to show a new engineering application for acoustic monitoring which could play a part in enabling the green transition while maintaining delicate ecosystems and enhancing energy security.

2. Taking stock of existing and planned infrastructure

The UK's current ORE infrastructure is primarily offshore wind turbines based in the South-East corner of the country where there are shallow waters, see Fig. 1. There have been rapid developments in offshore technology over the last decade with the maximum turbine capacity increasing from 2 MW to over 15 MW today. The average turbine capacity at sites under construction is currently a little over 9 MW (CES, 2024; TCE, 2024). As suitable, shallow near-shore sites have been built upon, newer developments have pushed further offshore where wind speeds and resultant energy production are higher, but water depths are deeper and conditions more hostile. Examining Fig. 1, one can see newer developments tend North off the Scottish coast or further offshore into the North Sea to the East. Having infrastructure further offshore in more hostile conditions raises energy security concerns and makes maintenance more challenging; both of these issues could be addressed through inexpensive instrumentation and remote sensing.

Table 1
Summary of current and planned offshore wind projects in the UK. Data from Crown Estate Scotland Spatial Hub (CES, 2024), OWF sites in England, Wales and Northern Ireland from The Crown Estate Open Data Portal (TCE, 2024), updated June 2025.

Status	Number of projects	Capacity
Decommissioned	1	4 MW
Active	51	13 900 MW
Under construction	9	7620 MW
Consented	13	3000 MW
Planning	49	47 400 MW

In 2024, the EU generated 62 TWh from offshore wind, while the UK alone generated a further 47 TWh. In 2024 alone, 2.6 GW of new capacity was installed in the EU+UK region (45% of which was in UK waters) (WindEurope, 2025). Notably, the average size of UK offshore wind farms under construction is now on the order of 1 GW; a substantial increase from the average size of currently operational wind farms at 0.3 GW (see Table 1). As turbines and farms increase in size so does the financial cost and complexity of installation, the potential environmental impacts on marine habitats, the effects of long-term cyclic wind and wave loading on turbine structural integrity and reliability, as well as our reliance on wind energy and associated grid stability. Instrumenting these sites can help us better understand these challenges whilst helping mitigate and minimise their impacts. This improved understanding represents a necessary step in realising The Crown Estate's stated goal of service life extension (TCE, 2022).

3. Detailed study into underwater acoustic sensing

A large number of UK Offshore Wind Farms (OWFs) are installed within or in the vicinity of Marine Protected Areas (MPAs), as shown in Fig. 1. Co-location of OWFs and MPAs has economic and ecological benefits (Ashley et al., 2018; Sanders et al., 2017), such as reducing the spatial conflict with other activities, enhancing biodiversity and increasing use by marine organisms during wind farm operation (Lindeboom et al., 2011; Inger et al., 2009), and deterring fishing activity such as bottom-towed fishing (dredging, trawling) which can be damaging to OWF infrastructure and seabed ecosystems. Examples of co-location of marine protected areas with active offshore wind farms in the UK are the West of Walney Marine Conservation Zone (MCZ), containing the Walney, West of Duddon, and Ormonde OWFs, and the Inner Dowsing, Race Bank, and North Ridge Special Area of Conservation (SAC), containing the Race Bank, Lynn and Inner Dowsing OWFs.

Research from Oceana revealed over 100,000 h of combined fishing activity from 907 UK and EU vessels in UK offshore MPAs in 2023, with over 33,000 h corresponding to bottom-towed fishing (Hammond, 2024). In this context, a key potential use for an acoustic sensing network is the detection and tracking of small to medium-sized vessels (e.g., fishing vessels) entering the MPA of a co-located wind-farm, whether they have a functioning AIS (Automatic Identification System) transponder or not. In order to choose a relevant site for our case study, we looked at OWFs at an advanced stage of development co-located with one of the MPA designation types that exist for UK waters, such as Marine Conservation Zones (MCZs), Special Areas of Conservation (SACs) with marine components, Marine Protected Areas (MPAs), and Nature Conservation MPAs (NCMPAs).

3.1. Case studies at Dogger Bank and Buchan Deep

Two sites were selected for case studies: first, Site A at Dogger Bank OWF, and second, Buchan Deep. These sites are marked on Fig. 1, and their bathymetry is shown in Fig. 2(a) and (b), respectively.

Dogger Bank site A was selected based on its advanced development stage (currently under construction), its location within an MPA (the Dogger Bank Special Area of Conservation, a 36,950 km^2 MPA designated to safeguard the subtidal sandbanks), and its unfavourable conservation status caused by bottom trawling (Appleby et al., 2020). An underwater acoustic sensing network would help with the efforts to implement vital management measures of fishing activities in this area.

The Dogger Bank OWF comprises three sites (A, B, C) with a combined capacity of 3688 MW and a total extent of 1408 km^2. Dogger Bank Site A is owned by Doggerbank Offshore Wind Farm Project 1 Projco Limited, a joint venture between SSE, Equinor and Vårgrønn. It is located off the North East coast of England, 130 km off the Yorkshire coast at 54°46′10″N, 1°54′32″E (approximate central point). The site is located in waters 20 to 60 m deep (see Fig. 2). It has a projected capacity of 1235 MW with an extent of 515 km^2. The development plan includes 95 GE Haliade-X turbines, each with 13 MW capacity. All sites in the Dogger Bank OWF will be developed as part of The Crown Estate's Round 3 lease program and are currently under construction.

Buchan Deep was selected for a second case study because it is the first deep-water site in the world to be exploited by commercial-scale floating wind turbines (JASCO, 2022). While the median depth at Dogger Bank is under 40 m, the Buchan Deep site is much deeper, with a median depth close to 100 m. As such, the two sites represent the extremes of likely OWF deployments between now and 2050. Further differences in bathymetry, sediment and sound speed profile will be discussed in detail below, before the resulting likely detection ranges at each site are shown. Buchan Deep is located 29 km off the Scottish coast at Peterhead, at 57°28′59.88″N, 1°21′0″W (approximate central location), and is owned by Equinor and Masdar, operating as Hywind (Scotland) Ltd. It has a maximum capacity of 30 MW, with an extent of 15.4 km^2. There are currently five turbines deployed over a 4 km^2 area, each with 6 MW capacity (Siemens SWT-6.0–154). In the present work, it is assumed that hydrophones can be mounted to a turbine foundation/substructure and that existing connections can be used for power and data transfer.

3.2. Modelling methodology

The likelihood of detecting acoustic emissions from a vessel can be estimated by considering the signal-to-noise ratio:

$$\mathrm{SNR}\,(f,r,z,\theta) = \mathrm{SL}\,(f) - \mathrm{PL}\,(f,r,z,\theta) - \mathrm{NL}\,(f)\,. \tag{1}$$

This varies as a function of frequency, f, as well as relative range, r, depth, z, and azimuth, θ, between the vessel and the sensor. SL is the source level (in dB re 1 μPa^2 Hz^{-1} @ 1 m) of the vessel's acoustic emissions, NL is the ambient noise level (in dB re 1 μPa^2 Hz^{-1}) at the sensor location, and PL is the propagation loss (in dB) between the vessel and sensor locations. We assume that a vessel is detectable when this ratio is above a reasonable threshold, e.g., $\mathrm{SNR}_{\min} = 10$ dB. Thus, a minimum detection range can be defined as the average range at which the desired threshold is attained:

$$r_{\min}\,(f,z,\theta) = \arg\min_{r}\left\{\left|\mathrm{SNR}\,(f,r,z,\theta) - \mathrm{SNR}_{\min}\right|\right\}. \tag{2}$$

A different model has been used to evaluate each of the terms in the SNR Eq. (1) for this study. Full details are given in the following Sections 3.2.1 and 3.2.2. Propagation Loss (PL) was modelled using the Range-dependent Acoustic Model (RAM) parabolic equation solver (Collins, 1993). This was operated using inputs from the General Bathymetric Chart of the Oceans (GEBCO) database for bathymetry (GEBCO, 2024), the Copernicus database (Copernicus, 2024b) for properties of the water column, and the Joint Monitoring Programme for Ambient Noise North Sea (JOMOPANS) methodology (de Jong et al., 2021b) for modelling the geo-acoustic properties of the North Sea sediment. The Source Level (SL) was estimated from the ECHO empirical model (MacGillivray and de Jong, 2021), and the noise level (NL) was predicted from the ambient noise model of Defence Research and Development Canada (DRDC) (Tollefsen and Pecknold, 2022), which considers noise caused by sea state, shipping, and rain. The different models employed have all been benchmarked and/or adopted by the community, and we have combined them, taking into account the variability of environment parameters, as presented in the following sections.

3.2.1. Geo-acoustic properties and propagation loss

The propagation loss $\mathrm{PL}\,(f,r,z,\theta)$ was modelled using a python implementation (PyRAM) of the RAM parabolic equation solver (Collins, 1993), which is valid for the frequency range of interest between 100 Hz and 10 kHz (Küsel and Siderius, 2019). The model propagates an acoustic source in range and depth and requires inputs describing: acoustic source depth and frequency; the sound speed profile(s) of the water column and sea-bottom; density and attenuation of the bottom sediment; and the bathymetry along the transect. Water volume absorption is not accounted for in PyRAM and was added during post-processing.

The acoustic field was sampled on a grid with a horizontal resolution of eight wavelengths (8λ) and a vertical resolution of 0.2λ, meaning the computed grid of propagation loss values was more densely populated with increasing frequency. Eight terms were used in the split-step Padé approximation.

The bathymetry was obtained from the General Bathymetric Chart of the Oceans (GEBCO) database (GEBCO, 2024) at a resolution of 15 arc-seconds (approximately 460 m at these latitudes) and is shown for the area surrounding both sites in Fig. 2. Sea-bottom depths were interpolated from these data along each transect at a resolution of 200 m (approximately twice the density of the GEBCO grid) originating at the locations specified in Table 2.

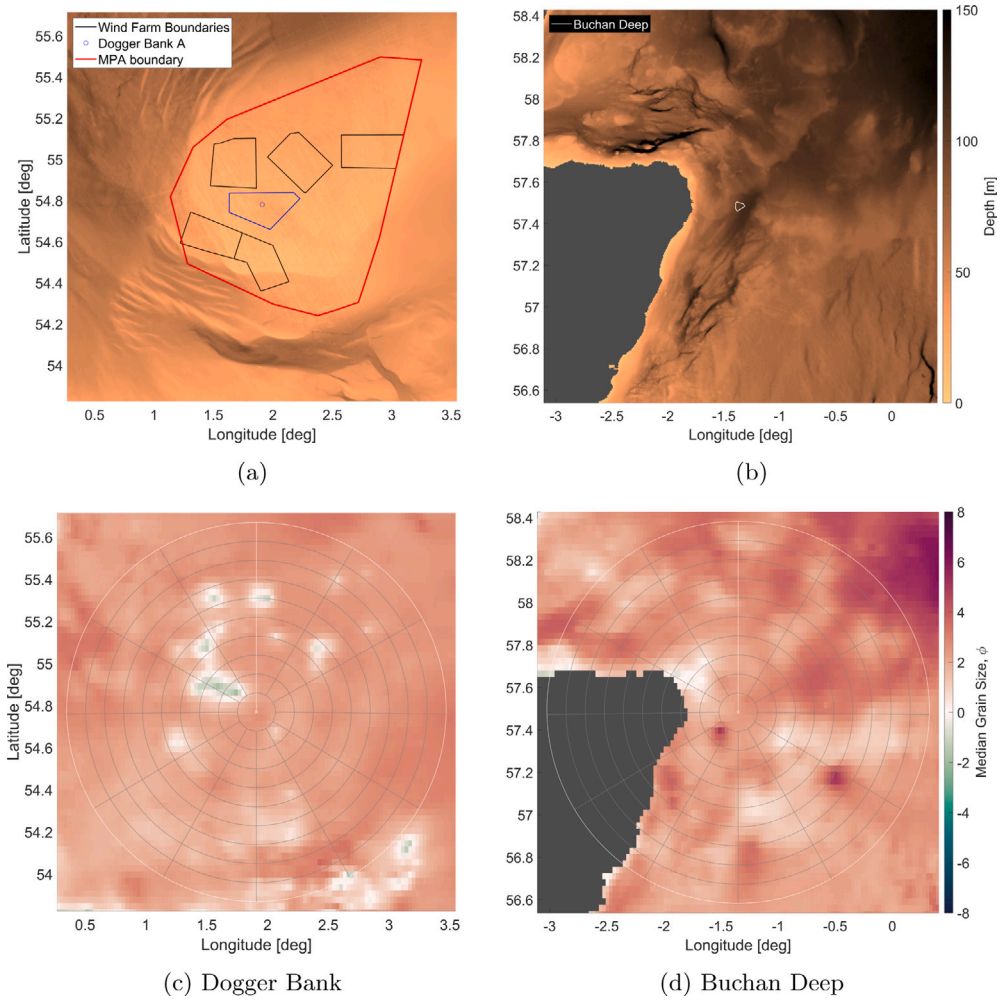

Fig. 2. Bathymetry (top row) and spatial variation of median grain size (bottom row) at Dogger Bank (left column) and Buchan Deep (right column) with range scale indicated by rings at 10 km increments from assumed source locations.

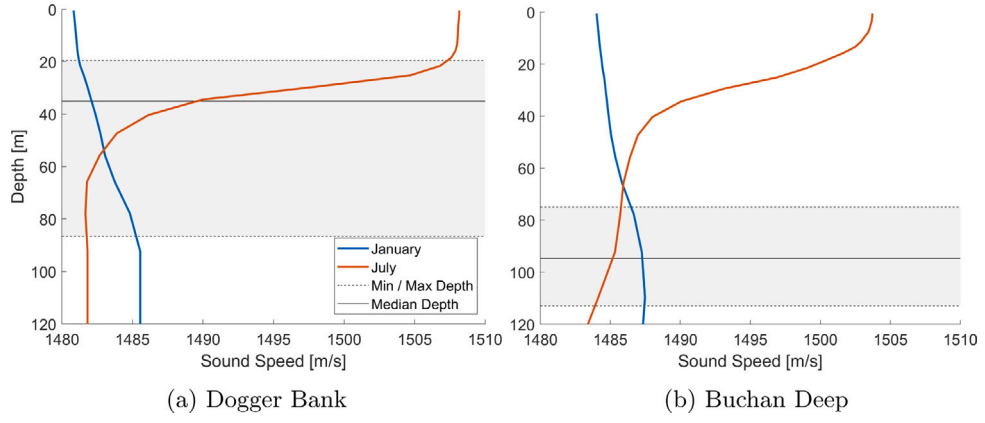

Fig. 3. Spatially averaged sound speed profiles over a 100 km radius for the year 2023 at the Dogger Bank (a) and Buchan Deep (b) ORE sites.

The monthly averages of salinity and temperature versus depth of the water column were obtained for the months of January (winter) and July (summer) from the Copernicus Marine Datastore (Global Ocean Physics Analysis and Forecast) at a grid resolution of 5 min (Copernicus, 2024b). The Mackenzie equation (Mackenzie, 1981) was used to calculate water sound speed profiles for all points within a 100 km radius of each site location. Median spatial profiles were calculated per month across these domains under the assumption of horizontal stationarity and are presented in Fig. 3. The sound speed profile (SSP) can be seen to exhibit significant temporal variability, varying from a near-constant sound speed of approximately 1485 m/s throughout the water column in winter to a downward refracting profile between 1482 m/s and 1508 m/s in summer.

The method used to determine acoustic properties of sediments followed the second version of the modelling by Nederlandse Organisatie voor Toegepast-natuurwetenschappelijk (TNO) under the JOMOPANS

Table 2
Modelled sediment parameters.

Site	Location	Percentile	Grain size $M(\phi)$	Density ratio ρ_s/ρ_w	Sound speed ratio $\nu(f) = c_s/c_w$	Attenuation $\beta(f)$ (dB/λ)
Dogger Bank	54°46′10″ N 1°54′32″ E	1st	−0.18	2.34	Aquarius 3	Aquarius 3
		50th	2.28	1.97	Aquarius 3	Aquarius 3
		99th	3.12	1.86	Aquarius 3	Aquarius 3
Buchan Deep	57°28′59″ N 1°21′00″ W	1st	0.37	2.25	Aquarius 3	Aquarius 3
		50th	2.34	1.97	Aquarius 3	Aquarius 3
		99th	4.36	1.72	Aquarius 3	Aquarius 3

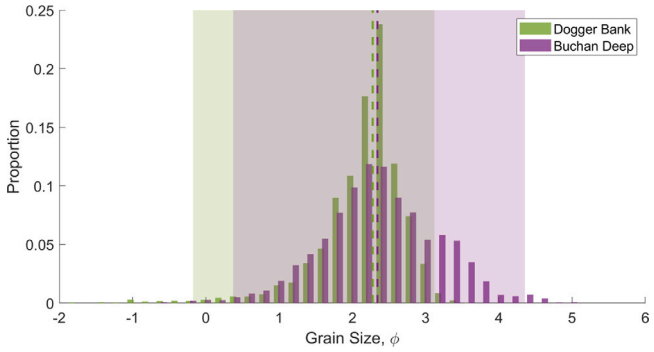

Fig. 4. Distribution of grain sizes within a 100 km radius of Dogger Bank and Buchan Deep with the 1st and 99th percentiles shown by the extent of the shaded region and the median indicated by the dashed line for each site. Percentile grain sizes are given in Table 2.

project (de Jong et al., 2021a). A volume absorption term was added to the PyRAM propagation loss output during post-processing using the empirical relationship presented by van Moll et al. (2009), which captures the effects of viscous absorption and chemical relaxation. To remain consistency with JOMOPANS methodology, water properties of $T = 10\,°C$, S = 34 ppt, $pH_{NBS} = 8$ and $z = 0$ m were used throughout (de Jong et al., 2021b). Sediment acoustic properties were functions of both frequency and source location grain size and assumed to be constant with range along each transect. The sediment grain sizes for Dogger Bank and Buchan Deep were evaluated by a linear interpolation of the grid of median grain size data from Bockelmann (2017) at the locations in Table 2.

Changes in median grain size, and hence sediment acoustic parameters, along each transect were investigated for the range of grain sizes present at each site. The propagation loss was modelled for homogeneous sediments of the 1st, 50th and 99th percentiles of the grain sizes found within a 100 km radius of the site. In addition, a spatially varying case was modelled with a range-dependent sea bottom where the grain size was directly interpolated from Bockelmann's grid along the transect. This approach extended the method of TNO which for each transect used only the grain size at the source location. In all cases, sediment properties at each range were assumed constant with depth. The grain sizes in the vicinity of both sites are shown in Fig. 2 and the associated distributions within 100 km radii are shown with the 1st, 50th and 99th percentiles in Fig. 4. The sediment density ratios for the respective grain sizes were obtained using the piecewise equation at the bottom of Table 4.18 in Ainslie (2010) and are summarised for each grain size case in Table 2.

Sound speed ratio (SSR) and attenuation were determined according to the Aquarius 3 model described in Section 3.7.3 of de Jong et al. (2021b). Aquarius 3 has a frequency and grain size dependent SSR fitted to absorption data from 12 sandy shallow measurement sites in Zhou et al. (2009), as given by

$$c_r(f) = \arctan\left(a \times \left(\log_{10}\left(\frac{f}{1000}\right) - b\right)\right) \times c + d \tag{3}$$

with coefficients: a = 1.7778, b = 0.4508, c = 0.000554 and d = 1.1208. The frequency dependence aimed to capture the deeper penetration of lower frequencies into higher density sediment and hence avoid overestimation of the propagation loss at low frequencies when fitting the model to ambient noise measurements in the North Sea (de Jong et al., 2021a). Absolute sediment sound speed values at each range along the transect, which were required for input to PyRAM, were attained by multiplying the SSR by the water sound speed interpolated to the bottom-depth at that range. The sediment sound speed profile was updated at each range where the bathymetry was defined (approximately every 200 m).

Frequency and grain size dependent attenuation was calculated according to

$$\beta(f) = \begin{cases} \beta_{HF}(\phi) & f > 1\,\text{kHz} \\ (f/1\,\text{kHz})^{0.8}\beta_{HF}(\phi) & f \leq 1\,\text{kHz} \end{cases} \tag{4}$$

where $\beta_{HF}(\phi)$ for the respective grain size was given by the equation at the bottom of Table 4.17 in Ainslie (2010).

A summary of the acoustic parameters of the sediments used for both sites are given in Table 2 and Fig. 5. Whilst the approach taken was consistent with the principal processing method presented by the JOMOPANS project, it should be noted that the Aquarius 3 model has not been verified or validated (Binnerts et al., 2021).

3.2.2. Source and noise levels

The source level characterises the acoustic emissions from a source as a mean square pressure level at a distance of 1 m from a hypothetical point (ISO 18405:2017). It can vary with a vessel's type, dimensions, and speed (Ross, 1979). The ECHO empirical model (MacGillivray and de Jong, 2021; de Jong et al., 2021b) was selected to predict the source power spectral density level (PSD). This model was chosen because it incorporates dependence on ship length and speed and is the only model that distinguishes between ship categories. The PSD was modelled for a 32 m fishing vessel travelling at 6.4 kn, which corresponds to the average measured length and speed of fishing vessels in the ECHO dataset and the result can be seen in Fig. 6.

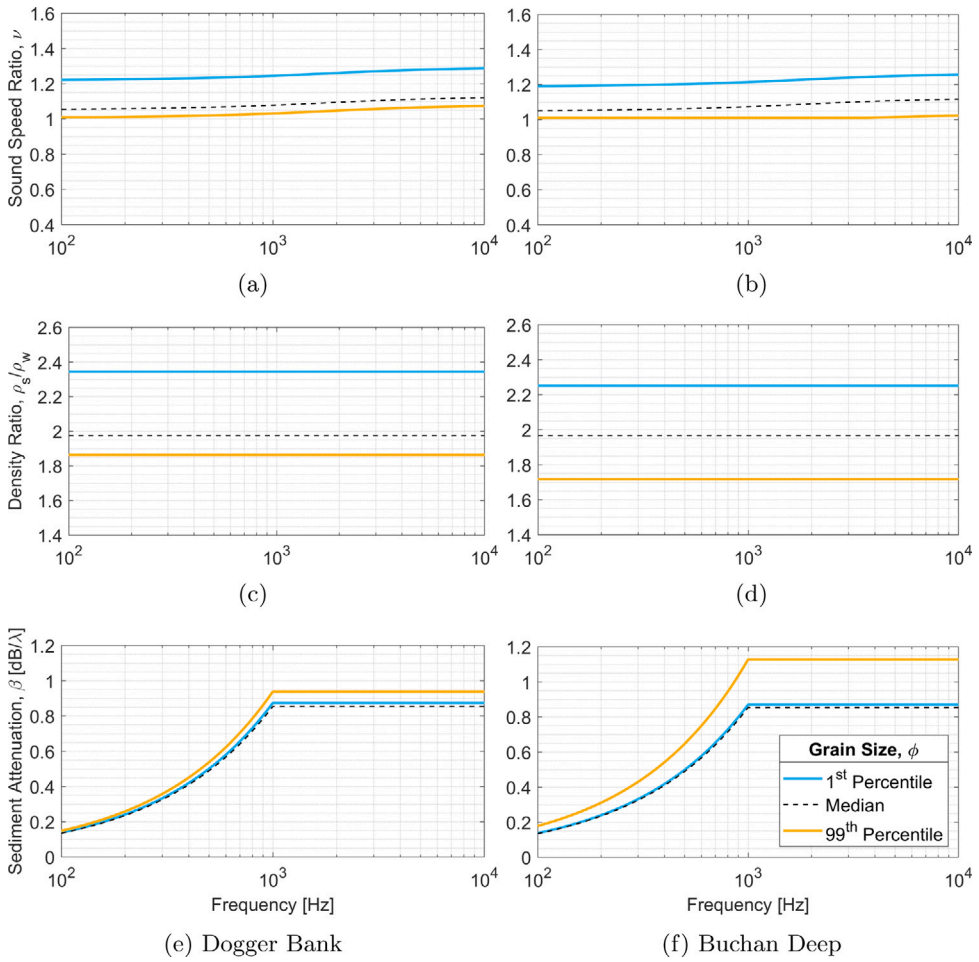

Fig. 5. Frequency dependent sediment sound speed ratio, density ratio and attenuation using the Aquarius 3 model for 1st, 50th and 99th percentile grain sizes at both ORE sites. Note that the acoustic parameter functions are not monotonic with grain size meaning the median may not necessarily lie between the 1st and 99th percentiles.

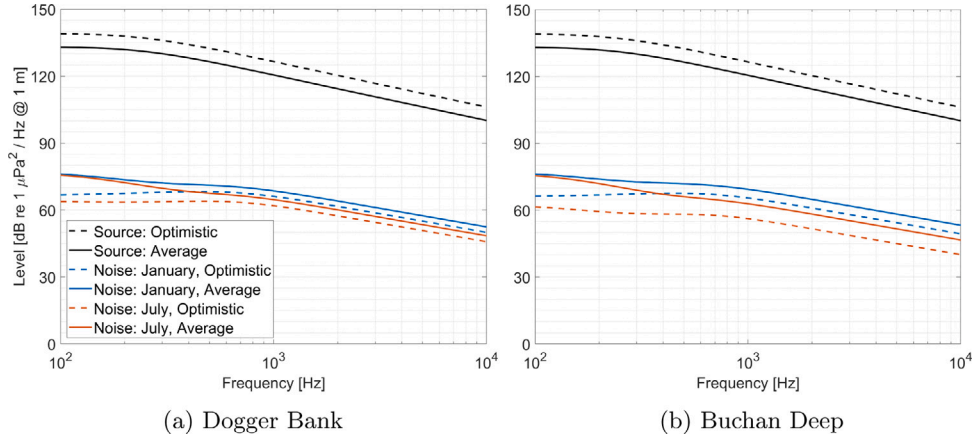

Fig. 6. ECHO ship source level spectrum for 32 m fishing vessel at 6.4 kn (solid black) with optimistic uncertainty bound of −6 dB (dashed black) and ambient noise for Dogger Bank (left) and Buchan Deep (right) using the model presented in Tollefsen and Pecknold (2022) with the parameters described in Table 3.

The noise level characterises unlocalised and continuous background acoustic emissions, including from natural sources, such as waves, wind, and rain, and anthropogenic sources, such as distant shipping. The frequency-dependent model presented by Tollefsen and Pecknold (2022) was selected as it allowed composite ambient noise spectra to be produced from simple definitions of noise sources such as wind speed, water depth and shipping level, which meant optimistic, average and pessimistic cases could be produced that had contextual meaning. The pessimistic case was neglected as it unsurprisingly did not result in a detection. Wind speed, alongside shipping level, was a primary driver of noise level between 100 Hz to 10 kHz, so the 25th and 50th percentile wind speeds at each site were calculated using the hourly sea-surface wind estimates for January and July 2024 from Copernicus (2024a). Eastward and northward wind speed

Table 3
DRDC ambient noise model input parameters per site, month and case with 25th, 50th and 75th percentile wind speeds from Copernicus (2024a). Equivalent WMO sea state tentatively derived from windspeed using the UK Met Office conversion table (Met Office, 2024).

Site	Month	Case	Wind speed [percentile]	Equivalent sea state	Shipping	Water depth	Rain rate
Dogger Bank	January	Optimistic	15.0 kn [25th]	3–4	'Low'	'Shallow'	None
		Average	19.9 kn [50th]	4	'Medium'	'Shallow'	None
Dogger Bank	July	Optimistic	9.2 kn [25th]	3	'Low'	'Shallow'	None
		Average	12.5 kn [50th]	3–4	'Medium'	'Shallow'	None
Buchan Deep	January	Optimistic	14.0 kn [25th]	3–4	'Low'	'Shallow'	None
		Average	21.8 kn [50th]	4–5	'Medium'	'Shallow'	None
Buchan Deep	July	Optimistic	4.8 kn [25th]	2	'Low'	'Shallow'	None
		Average	10.2 kn [50th]	3	'Medium'	'Shallow'	None

components (at 10 m above the surface) were combined to find the wind speed magnitude. These resulted in the input parameters to the DRDC model for each site, month and case shown in Table 3. The ambient noise spectra for both ORE sites and cases are shown in Fig. 6.

4. Results

Examples of the modelled propagation losses at Buchan Deep and Dogger Bank ORE sites are shown in Figs. 7(a) and 7(b) for a selection of frequencies: 250 Hz, 500 Hz, 1 kHz, 2 kHz and 5 kHz. These show the variation with depth and range over a Northward azimuthal transect in January and July with a sediment of range-dependent grain size. Propagation conditions were more favourable in January than July at both sites across the full water column. Buchan Deep also had more favourable conditions than Dogger Bank with greater propagation distances clearly visible, particularly in July where a channel between 20 m and the bottom is present beyond 60 km. Overall, these examples illustrate that there is little variation in propagation loss with depth and justify the depth averaging within the following analysis.

The detectability of a typical fishing vessel in the vicinity of each ORE site is shown across Figs. 8(a) and 8(b) for average and optimistic detection conditions and both range-dependent and range independent sediment types. The black line indicates the frequency dependent detection range that is the mean distance between the nearest and furthest distances at which the SNR crosses below the threshold (SNR_{min}). The range between the nearest and furthest crossings of the threshold is indicated by the shaded grey area (this range is often zero and therefore not always visible). The detection range for a single transducer with an assumed detection threshold of 10 dB is approximately 200 m in winter and 300–400 m in summer for the average case, and rises to approximately 1 km and 3 km, respectively, for the optimistic case. It can be seen across all sites and months that larger grain sizes (lower M) result in greater detection ranges and these larger grain sizes favour lower frequencies more than smaller grain sizes. The detection range of the range-dependent (interpolated) sediment closely matches the range-independent median grain size sediment for all cases. For the following results the range-dependent (interpolated) sediment was used unless stated otherwise.

Greater detection ranges can be seen in summer at both sites with optimal frequencies from 1 to 3 kHz at Buchan Deep and 1.5 to 4 kHz at Dogger Bank. There is a more substantial increase in detection range at Buchan Deep of approximately 2.2 km between winter and summer than at Dogger Bank (0.8 km), though this increase is skewed towards higher frequencies.

Figs. 9 and 10 show the azimuthal variation in SNR and detection range under optimistic conditions at Dogger Bank and Buchan Deep, respectively. The performance is shown for a selection of representative frequencies within the optimal detection bandwidth (500 Hz, 1 kHz, 2 kHz). While there is minimal variation over azimuth, there is a notable drop in SNR at Buchan Deep around 12 km away from the site on a bearing of N220 which corresponds to a region of considerably finer sediment that can be seen in Fig. 2.

5. Discussion

The results above give an example of the range over which a typical fishing vessel might be detected using a single hydrophone in two different offshore wind farm locations. Typical 'average' detection ranges were found to be in the region of 300–400 m, while the optimistic cases gave a range of 2–4 km. Optimal detection frequencies for the exemplar vessel chosen were typically in the range of 500 to 5 kHz.

The detection range is highly sensitive to the ambient noise estimate chosen, which has a high degree of variability (see Fig. 6). Furthermore, the ambient noise was found to be high at the two sites chosen, especially in winter, when rough sea states are expected even on an 'average' day. The analysis in this paper also neglects the possibility of tones from a vessel that are louder than the broadband noise (a conservative assumption inherent in the JOMOPANS-ECHO model (de Jong et al., 2021b; MacGillivray and de Jong, 2021)). The presence of tones would improve detectability of vessels over the ambient noise.

As well as high ambient noise, the relatively small detection ranges were affected by high propagation loss (see Figs. 7(a) and 7(b)). This result appears to be due to a combination of highly attenuating sediment and downward refracting conditions, which coupled together to give a significantly higher propagation loss than either would in isolation.

Seasonal variability in detection range was found at both sites, with higher propagation loss in July, but lower ambient noise leading to an increased overall detection range expected in the Summer than the Winter.

The two example sites were chosen as a representative shallow site within an existing MPA (Dogger Bank A), and a deep site which is similar to those that will be exploited more in future as floating wind farms become commonplace (Buchan Deep). The similarities between the results (Figs. 8(a) and 8(b)) at the two sites suggests that water depth has only a limited impact on the detection range over the frequencies of interest.

The detection range is highly dependent on seabed sediment properties. There are two major sources of uncertainty in the modelling of propagation loss in seabed sediment: first, the actual composition of the seabed is only mapped with a resolution of 1 × 1 nautical miles, and there is uncertainty and inconsistency in the mapping methods (Bockelmann et al., 2018), and, second, models for the acoustic properties of sediment contain many assumptions and are not typically well-validated — see Section 3.2.1. The effect of grain size on propagation loss can be seen Fig. 8(a). For example, for the July optimistic case (right-hand column), the range at a given frequency can vary by over 100%, and the optimal frequency can shift between 200 Hz and from 5 kHz depending on grain size. Across all the cases in Figs. 8(a) and

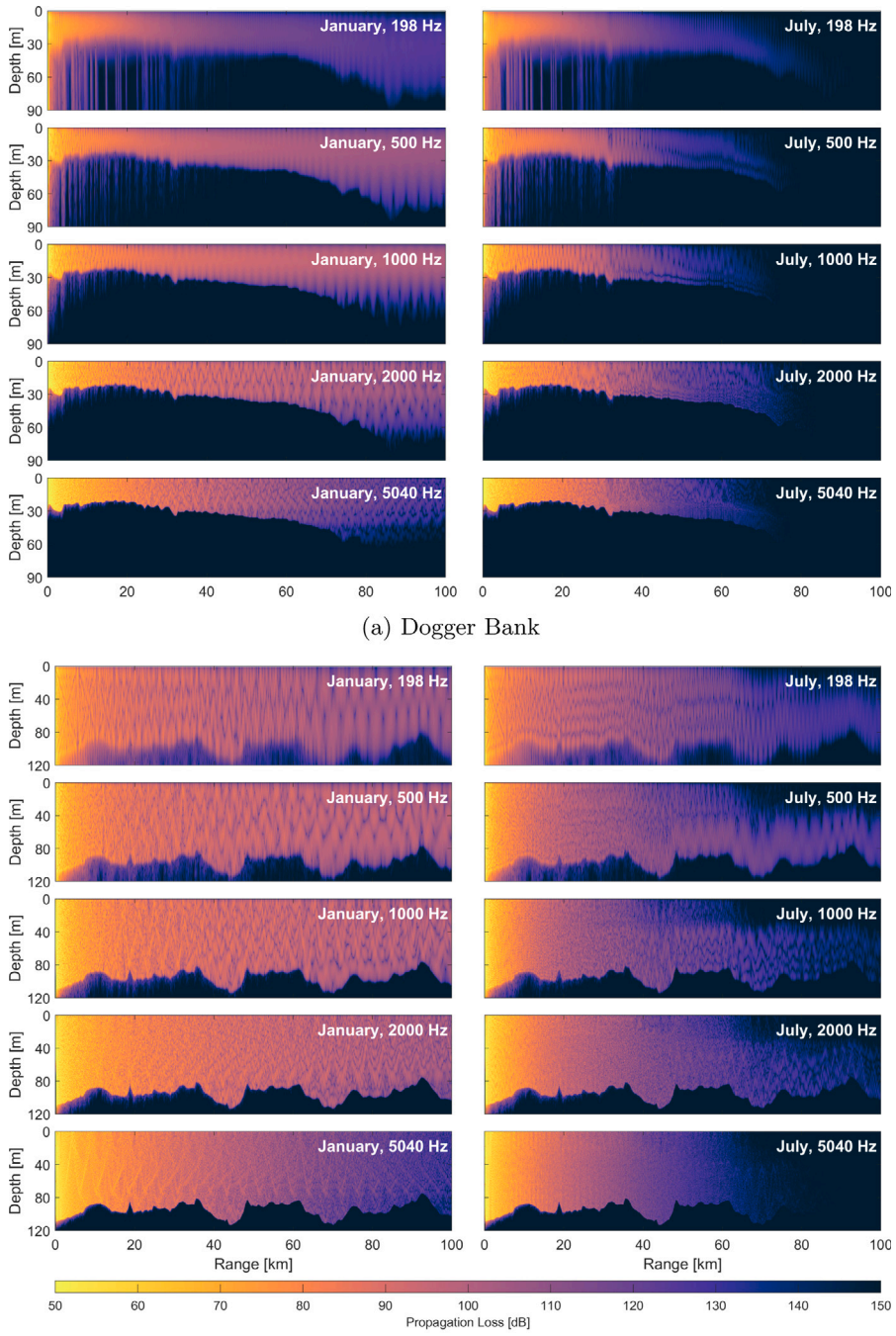

Fig. 7. Selection of propagation loss profiles using a range-dependent sediment profile at 200 Hz (top row) to 5 kHz (bottom row) along a 100 km Northward transect at the Dogger Bank (a) and Buchan Deep (b) ORE sites during January (left column) and July (right column).

8(b), it can be seen that considering the actual grain size at each range location gives a result very similar to that obtained using the median grain size (range-independent). Given the existing uncertainty in the sediment properties and behaviour, this result suggests that effort can be saved by using a range-independent grain size.

For optimal farm performance, offshore wind turbines are typically spaced 7–10 rotor diameters apart (Burton et al., 2021). The devices installed at Dogger Bank A (GE Haliade-X 13 MW (TCE, 2024)) have a 220 m diameter, suggesting a spacing of 1.5 to 2.2 km. The slightly smaller devices at Buchan Deep (154 m diameter, Siemens SWT-6.0-154 (CES, 2024)) mean that the spacing is likely to be 1.0 to 1.5 km. These distances are towards the upper end of the detection ranges found across the cases tested in this work, suggesting that signal processing enhancement may be necessary for monitoring activity across the whole area covered by the turbines. Monitoring of an MPA that extends over a much greater area than that of the wind farm (as is the case for Dogger Bank A) is unlikely to be feasible using solely turbine-mounted instruments. Future work could consider the use of autonomous vehicles (e.g. gliders), which dock at wind farms to recharge but are able to monitor a larger area.

This study has shown the feasibility of using hydrophones to detect activity around offshore wind turbines, but more detailed modelling

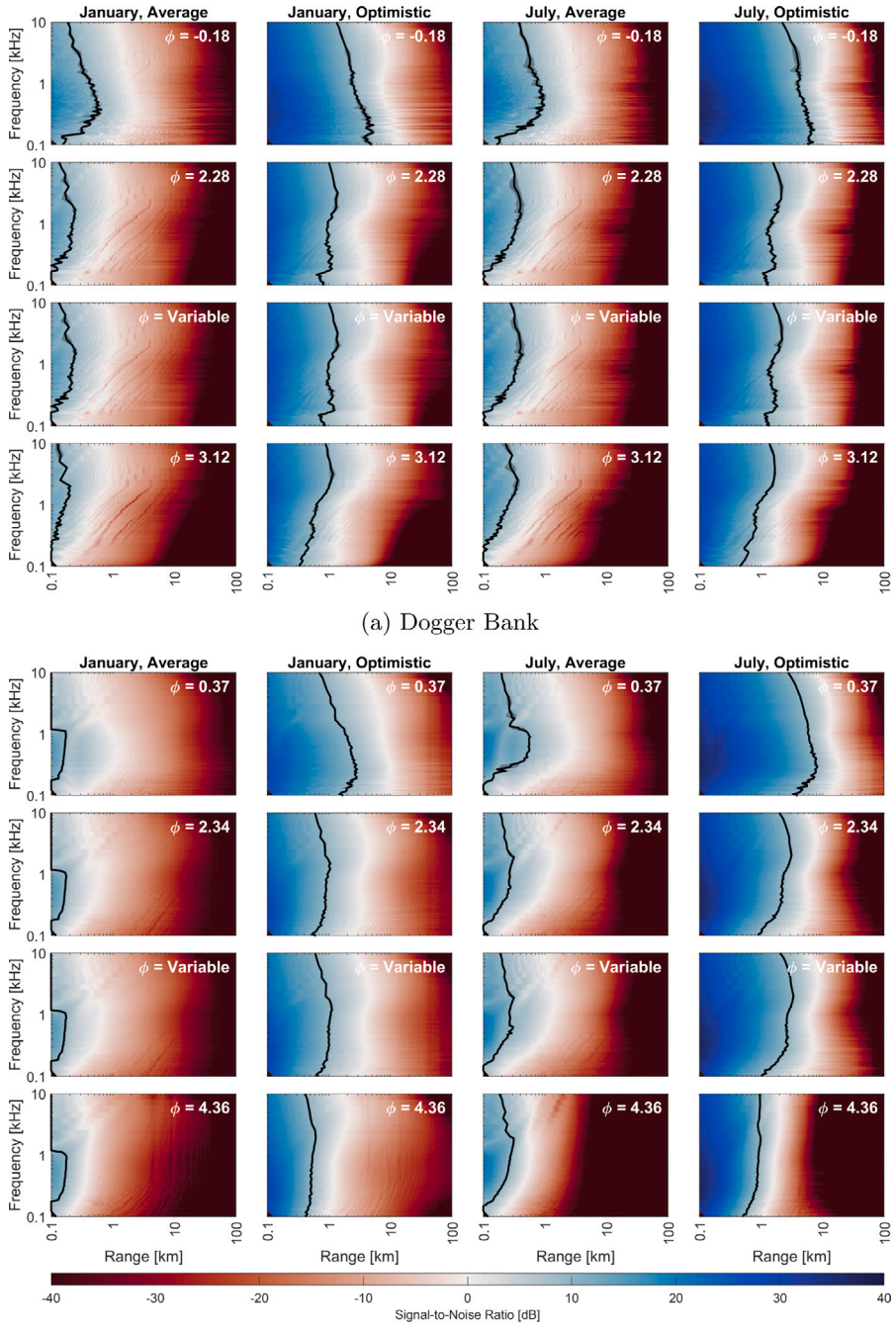

(a) Dogger Bank

(b) Buchan Deep

Fig. 8. Depth-averaged SNR and detection ranges (SNR ≥ 10 dB), indicated by the black line, for a Northward transect from the Dogger Bank (a) and Buchan Deep (b) ORE sites. Variation shown in: grain size — coarsest 1st percentile (top), 50th percentile, range-dependent, and 99th percentile (bottom); winter versus summer; and average versus optimistic conditions.

would be required to understand the uncertainties in detection ranges. For example, a stochastic study (e.g. Monte Carlo) of the different parameters of the sediment, sound speed profile, noise, and source levels could be undertaken.

While the study has focussed on two particular wind farms and one example application (detection of illegal fishing), the method could be extended to different kinds of offshore infrastructure (e.g. oil and gas installations) and to alternative acoustic sources (e.g. marine mammals, military craft). Furthermore, the approach could be repeated at any geographical location for which the seabed properties are known.

6. Conclusions

This paper has explored the potential benefits of installing acoustic sensors on ORE infrastructure. The use case of detecting illegal fishing activity near wind turbines has been studied at two example sites: Dogger Bank A and Buchan Deep.

The source sound level, ambient noise, sound speed profile and seabed properties have all been found from existing models and databases, and the well-established Range-dependent Acoustic Model used to estimate the propagation loss. The results show that a single

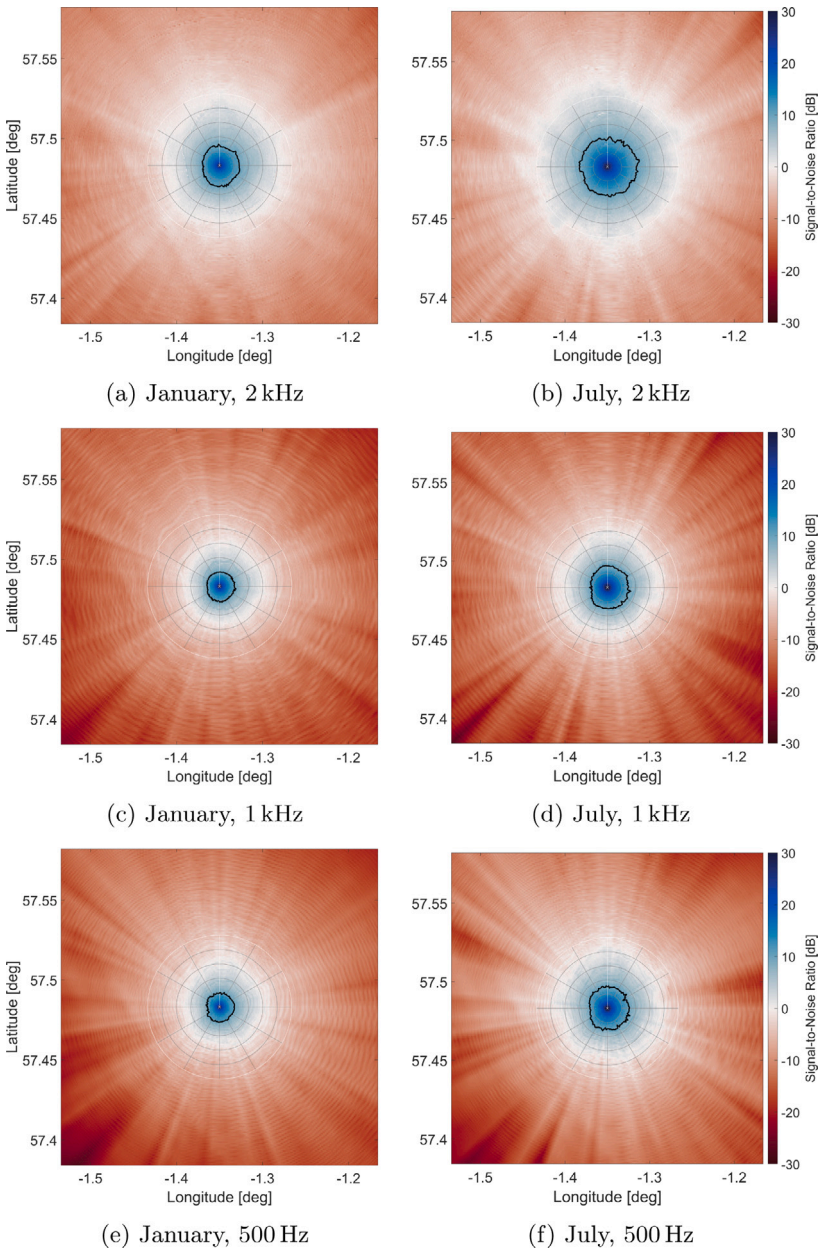

Fig. 9. Dogger Bank ORE site: depth-averaged SNR estimates with azimuth using the range-dependent sediment model under optimistic conditions during winter (left column) and summer (right column) for three representative frequencies of 500 Hz (bottom row), 1 kHz (middle row), and 2 kHz (top row). The black line shows the detection range (SNR $\geq$ 10 dB) and the grey circles represent increments of 1 km in range.

hydrophone would be likely to detect a typical fishing vessel at ranges of 300–400 m in the average case, up to 2 km under favourable conditions. These estimates are highly dependent on sediment properties and ambient noise, but water depth appears to have little impact on detection range. Furthermore, the downward-refracting sound speed profile in the Summer, in combination with highly attenuating sediment causes a significant increase in propagation loss at both sites compared with the Winter result. This increase in propagation loss is more than compensated for by a reduction in ambient noise in the summer (due to calmer sea states), such that the detection range is increased in the Summer.

The optimistic detection ranges are comparable to or slightly exceed typical turbine spacing, suggesting that if a hydrophone was mounted on every turbine in a wind farm, monitoring of fishing activity could take place over most or all of the area covered by the farm, but not beyond the extent of the turbines into a wider Marine Protected Area.

Future work should explore the use of hydrophone arrays, which would require a detailed study into signal coherence to enable advanced processing techniques such as beamforming for improved directionality and range. Additionally, the consideration of louder tonal signals, which are typically emitted by vessel engines, could extend the detection range. Deployment strategies should consider various configurations: sensors mounted directly on infrastructure, tethered systems on the seabed or in the water column, and mobile units that roam around installations. Broader system design could involve intra- and inter-farm acoustic networks, with potential for multi-use of existing fibre optic cables to support both data transmission and acoustic sensing. Beyond illegal fishing detection, acoustic sensors could support a range of applications including underwater noise monitoring for regulatory compliance, marine mammal conservation through vocalisation tracking, surveillance for energy security, and structural health monitoring of offshore infrastructure.

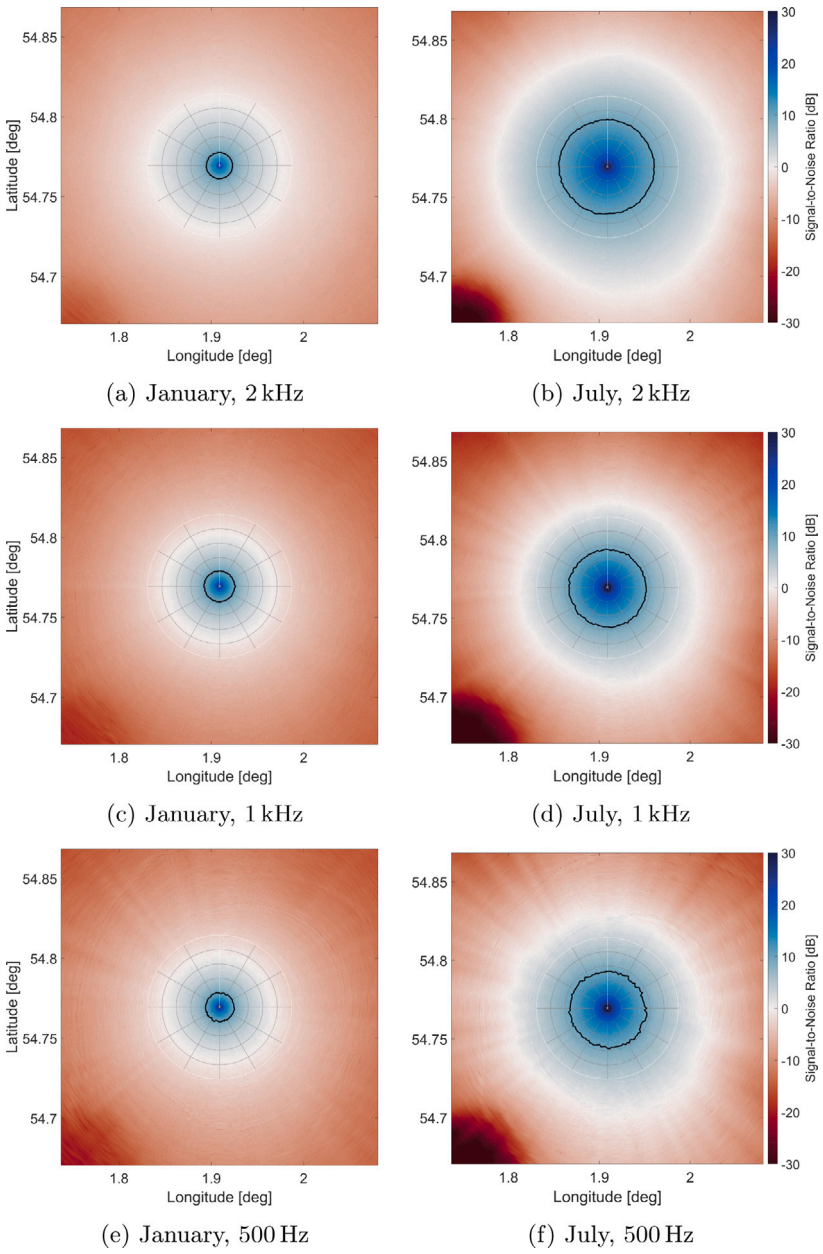

(a) January, 2 kHz (b) July, 2 kHz

(c) January, 1 kHz (d) July, 1 kHz

(e) January, 500 Hz (f) July, 500 Hz

Fig. 10. Buchan Deep ORE site: depth-averaged SNR estimates with azimuth using the range-dependent sediment model under optimistic conditions during winter (left column) and summer (right column) for three representative frequencies of 500 Hz (bottom row), 1 kHz (middle row), and 2 kHz (top row). The black line shows the detection range (SNR $\geq$ 10 dB) and the grey circles represent increments of 1 km in range.

CRediT authorship contribution statement

Magnus Ferris: Writing – original draft, Investigation. **Edward Clark:** Investigation. **Guillermo Jiménez Arranz:** Investigation. **Philippe Blondel:** Writing – review & editing, Supervision, Funding acquisition. **Cormac Reale:** Writing – review & editing, Writing – original draft, Supervision, Funding acquisition. **Alan Hunter:** Writing – review & editing, Writing – original draft. **Anna Young:** Writing – review & editing, Writing – original draft, Supervision, Funding acquisition, Conceptualization.

Declaration of competing interest

The authors declare that they have no known competing financial interests or personal relationships that could have appeared to influence the work reported in this paper.

Acknowledgements

This project was funded by the UK Acoustics Network (UKAN+) under UKRI grant EP/V007866/1. The authors also acknowledge funding from the University of Bath Beacon in Zero Carbon Offshore Renewable Energy, led by Anna Young.

References

Ainslie, M.A., 2010. Principles of Sonar Performance Modelling. Springer Berlin Heidelberg, Germany, http://dx.doi.org/10.1007/978-3-540-87662-5.

Appleby, T., Condon, J., Rammelt, T., Reuchlin-Hugenholtz, E., Solandt, J.-L., 2020. Report to Inform Appropriate Assessment of Fishing Operations on the Dogger Bank SACs. Technical report, Blue Marine Foundation, WWF, Client Earth & Marine Conservation Society, https://www.bluemarinefoundation.com/wp-content/uploads/2020/09/Dogger-Bank-Report-Final.pdf.

Ashley, M., Austen, M., Rodwell, L., Mangi, S.C., 2018. Co-locating offshore wind farms and marine protected areas: A United Kingdom perspective. In: Offshore Energy and Marine Spatial Planning. Routledge, Oxon, UK, pp. 246–259.

Bald, J., 2022. Reviewing the ecological impacts of offshore wind farms. Npj Ocean. Sustain. (1).

Binnerts, B., de Jong, C.A.F., von Benda-Beckmann, S., de Krom, P., Östberg, M., Folegot, T., Ainslie, M., Welch, S., 2021. Model predictions 2018 measurement sites. https://northsearegion.eu/media/17955/wp4_t43_report_2018_modelpredictionsandupdates_final.pdf.

Bockelmann, F.-D., 2017. Median Grain Size of North Sea Surface Sediments. World Data Center for Climate (WDCC) at DKRZ, http://dx.doi.org/10.1594/WDCC/coastMap_Substrate_MGS.

Bockelmann, F.-D., Puls, W., Kleeberg, U., Müller, D., Emeis, K.-C., 2018. Mapping mud content and median grain-size of North Sea sediments – A geostatistical approach. Mar. Geol. 397, 60–71. http://dx.doi.org/10.1016/j.margeo.2017.11.003.

Burton, T., Jenkins, N., Bossanyi, E., Sharpe, D., Graham, M., 2021. Wind Energy Handbook, third ed. John Wiley & Sons, Inc., Hoboken, NJ.

CES, 2024. Crown estate Scotland spatial hub. (Accessed 15 March 2024). https://crown-estate-scotland-spatial-hub-coregis.hub.arcgis.com/.

Collins, M.D., 1993. A split-step Padé solution for the parabolic equation method. J. Acoust. Soc. Am. 93 (4), 1736–1742. http://dx.doi.org/10.1121/1.406739, (Accessed 01 September 2022).

Copernicus, 2024a. Global Ocean Hourly Reprocessed Sea Surface Wind and Stress from Scatterometer and Model. http://dx.doi.org/10.48670/MOI-00185, https://resources.marine.copernicus.eu/product-detail/WIND_GLO_PHY_L4_MY_012_006/INFORMATION.

Copernicus, 2024b. Global ocean physics analysis and forecast. http://dx.doi.org/10.48670/moi-00016, (Accessed 15 March 2024). https://data.marine.copernicus.eu/product/GLOBAL_ANALYSISFORECAST_PHY_001_024/description.

de Jong, C.A.F., Binnerts, B., Östberg, M., Karasalo, I., Folegot, T., Clorennec, D., Ainslie, M., MacGillivary, A., Warner, G., Wang, L., 2021a. Jomopans model benchmarking and sensitivity studies. https://northsearegion.eu/media/17954/wp4_t42_report_modelverification_final.pdf.

de Jong, C., Binnerts, B., Robinson, S., Wang, L., 2021b. Guidelines for modelling ocean ambient noise. Rep. EU INTERREG Jt. Monit. Program. Ambient Noise North Sea (JOMOPANS).

GEBCO, 2022. The GEBCO 2022 grid. (Accessed 15 March 2024). https://www.gebco.net/data_and_products/gridded_bathymetry_data/gebco_2022/.

GEBCO, 2024. GEBCO 2023 grid. http://dx.doi.org/10.5285/f98b053b-0cbc-6c23-e053-6c86abc0af7b, https://www.gebco.net/data_and_products/gridded_bathymetry_data/.

GOV.UK, 2022. British energy security strategy. (Accessed 15 March 2024). https://www.gov.uk/government/publications/british-energy-security-strategy/british-energy-security-strategy#renewables.

Hammond, A., 2024. Death by a Thousand Cuts: Bottom-Trawl Fishing in UK Offshore Marine Protected Areas. Technical report, https://uk.oceana.org/wp-content/uploads/sites/14/2024/05/Bottom-trawl-fishing-in-offshore-UK-MPAs_Ocean-briefing-March-2024-1-1.pdf.

Inger, R., Attrill, M.J., Bearhop, S., Broderick, A.C., James Grecian, W., Hodgson, D.J., Mills, C., Sheehan, E., Votier, S.C., Witt, M.J., et al., 2009. Marine renewable energy: potential benefits to biodiversity? An urgent call for research. J. Appl. Ecol. 46 (6), 1145–1153.

JASCO, 2022. Hywind Scotland Floating Offshore Wind Farm: Sound Source Characterisation of Operational Floating Turbines. Technical report, https://cdn.equinor.com/files/h61q9gi9/global/f7e7b24cd5d4291a0c7ebb7eb17baa83f452a513.pdf?equinor-hywind-scotland-sound-source-characterisation.pdf.

JNCC, 2023. UK offshore marine protected areas. (Accessed 15 March 2024). https://hub.jncc.gov.uk/assets/ade43f34-54d6-4084-b66a-64f0b4a5ef27.

Küsel, E.T., Siderius, M., 2019. Comparison of Propagation Models for the Characterization of Sound Pressure Fields. IEEE J. Ocean. Eng. 44 (3), 598–610. http://dx.doi.org/10.1109/JOE.2018.2884107.

Lindeboom, H.J., Kouwenhoven, H., Bergman, M., Bouma, S., Brasseur, S., Daan, R., Fijn, R., De Haan, D., Dirksen, S., Van Hal, R., et al., 2011. Short-term ecological effects of an offshore wind farm in the Dutch coastal zone; a compilation. Environ. Res. Lett. 6 (3), 035101.

MacGillivray, A., de Jong, C., 2021. A reference spectrum model for estimating source levels of marine shipping based on Automated Identification System data. J. Mar. Sci. Eng. 9 (4), 369.

Mackenzie, K.V., 1981. Nine-term equation for sound speed in the oceans. J. Acoust. Soc. Am. 70 (3), 807–812.

Met Office, 2024. Beaufort wind force scale. https://www.metoffice.gov.uk/weather/guides/coast-and-sea/beaufort-scale.

Prendergast, L., Reale, C., Gavin, K., 2018. Probabilistic examination of the change in eigenfrequencies of an offshore wind turbine under progressive scour incorporating soil spatial variability. Mar. Struct. 57, 87–104.

Ross, D., 1979. Mechanics of Underwater Noise. Pergamom Press.

Sanders, N., Haynes, T., Goriup, P.D., 2017. Marine protected areas and offshore wind farms. In: Management of Marine Protected Areas: A Network Perspective. Wiley Online Library, New Jersey, USA, pp. 263–280.

TCE, 2022. Offshore Wind Report 2022. (Accessed 15 March 2024). https://www.thecrownestate.co.uk/media/4382/11720_owoperationalreport_2022_tp_020523plusaccessibility.pdf.

TCE, 2024. The crown estate data portal. (Accessed 15 March 2024). https://opendata-thecrownestate.opendata.arcgis.com/.

Tollefsen, C.D.S., Pecknold, S., 2022. A Simple Yet Practical Ambient Noise Model. Technical Report DRDC-RDDC-2022-D051, Defence Research and Development Canada.

van Moll, C.A.M., Ainslie, M.A., van Vossen, R., 2009. A Simple and Accurate Formula for the Absorption of Sound in Seawater. IEEE J. Ocean. Eng. 34 (4), 610–616. http://dx.doi.org/10.1109/JOE.2009.2027800, Conference Name: IEEE Journal of Oceanic Engineering. (Accessed 29 October 2024).

WindEurope, 2025. Wind energy in Europe: 2024 statistics and the outlook for 2025–2030. https://windeurope.org/intelligence-platform/product/wind-energy-in-europe-2024-statistics-and-the-outlook-for-2025-2030.

Zhou, J.-X., Zhang, X.-Z., Knobles, D.P., 2009. Low-frequency geoacoustic model for the effective properties of sandy seabottoms. J. Acoust. Soc. Am. 125, 2847–2866. http://dx.doi.org/10.1121/1.3089218.